Microwave Radar-Based Breast Cancer Detection: Imaging in Inhomogeneous Breast Phantoms

M. Klemm, *Member, IEEE*, J. A. Leendertz, D. Gibbins, I. J. Craddock, A. Preece, and R. Benjamin

***Abstract*—This letter presents, for the first time, experimental work on microwave breast cancer imaging using inhomogeneous breast phantoms. A recently designed 31-antenna array is used in imaging experiments. The imaging system operates in the full ultrawideband frequency range, between 3 and 10 GHz. To verify imaging performance of our system, new breast phantoms with inhomogeneous interior were developed. For three different breast phantoms presented in this work, the contrast between spherical phantom tumors and surrounding materials ranges from 5:1 to 1.6:1. Our results show that the biggest challenge in radar microwave imaging is the inhomogeneity of the volume being sensed, and not the contrast itself. In addition to experimental results, we also present the new image formation algorithm, which is a modified version of the delay-and-sum (DAS) algorithm. The new algorithm makes use of a new weighting factor, the coherence factor. The new algorithm is effective in reducing clutter, providing better images. For the most demanding imaging example presented herein, the new algorithm improves the peak clutter-to-target energy ratio by 3.1 dB.**

***Index Terms*—Antenna array, biomedical electromagnetic imaging, medical imaging, microwave imaging, radar imaging.**

I. Introduction

THE most recently published data on electromagnetic (EM) properties of breast tissues [1] suggest that the contrast between healthy and malignant tissues might be significantly lower and also that the breast interior is more inhomogeneous than indicated by previously published data (e.g., [2]). This most recent report disclosing a more challenging case for microwave breast imaging than previously thought resulted in a development of realistic *numerical* breast phantoms based on magnetic resonance imaging (MRI) [3], [4]. However, to the best of our knowledge, *experimental* imaging using realistically inhomogeneous breast phantoms has not been attempted yet. The most advanced curved breast phantom for microwave imaging, composed of homogeneous materials, has recently been presented in [5].

In this letter, we present microwave radar-based breast imaging in inhomogeneous phantoms. These phantoms do not attempt to be as realistic as the numerical ones (which might be impossible in practice). However, they are the next step forward in the development of more realistic phantoms for experimental microwave imaging research. In addition, we also present a new image formation algorithm, which is a modified version of the delay-and-sum (DAS) algorithm. The new algorithm makes use of a new weighting factor, the coherence factor, previously also applied in ultrasound imaging.

Manuscript received July 23, 2009; revised September 10, 2009 and October 08, 2009. First published November 17, 2009; current version published January 08, 2010.

The authors are with the Centre for Communications Research, Department of Electrical and Electronic Engineering, University of Bristol, Bristol BS8 1UB, U.K. (e-mail: m.klemm@bristol.ac.uk).

Color versions of one or more of the figures in this letter are available online at http://ieeexplore.ieee.org.

Digital Object Identifier 10.1109/LAWP.2009.2036748

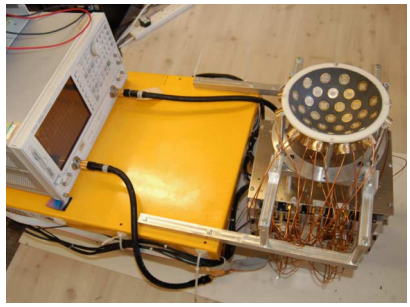

Fig. 1. Microwave radar-based imaging system.

II. 3D Radar Imaging Setup

A. Measurement Setup

The complete description of the radar microwave imaging system we have developed can be found in [5] and [6]. However, the system presented in this work uses a newly designed 31-antenna array, presented in [7]. For completeness, a brief description of the imaging measurement procedure is presented in the following.

In the measurement setup, the array is connected with coaxial cables to a custom-built network of electromechanical switches. The bank of switches selects all possible pairs of antennas within the array and connects them in turn to a vector network analyzer (VNA; Rohde&Schwarz ZVB20), which performs the radar measurement in the frequency domain (S_{21} in this case). In a post-reception step, all measured data are transformed into the time domain. With 31 antennas in the array, 465 independent measurements (multistatic radar signals) are recorded. A computer controls both the VNA and the switch bank, and the measurement takes about 80 s to complete. Recorded radar signals serve as an input to the image formation (beamforming) algorithm, described later in Section III. The complete experimental imaging system is presented in Fig. 1.

During measurements, antennas are immersed in a matching liquid to reduce reflections from the skin and for a more compact antenna design. We decided that the matching liquid would be the same as the material-simulating properties of normal breast fat, mainly for practical reasons (only one liquid required). This liquid [8] has a relative dielectric constant of about 10 and attenuation of 0.8 dB/cm at 3 GHz. This material is also dispersive.

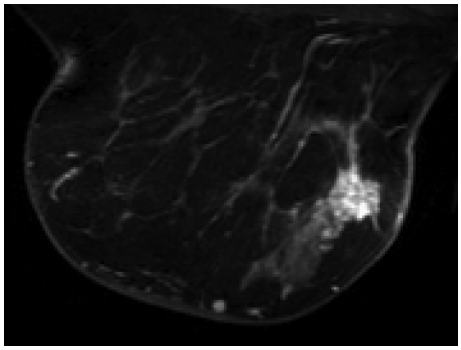

Fig. 2. Contrast-enhanced MRI image through the breast. Tumor visible on the right-hand side, as well as dense tissues scattered throughout the breast.

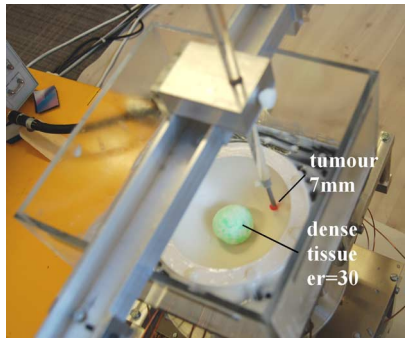

Fig. 3. Setup of the imaging experiment 1.

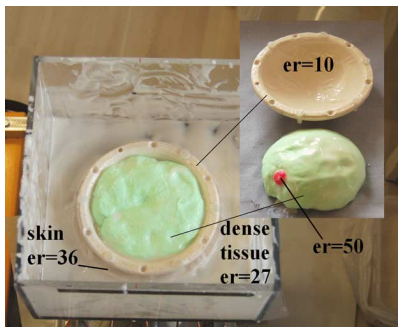

Fig. 4. Setup of the imaging experiment 2.

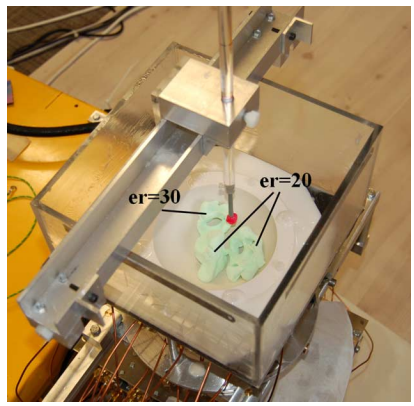

Fig. 5. Setup of the imaging experiment 3.

B. 3D Breast Phantoms for Microwave Imaging

For experimental testing, we developed appropriate materials and a 3D breast phantom. The phantom is similar to the one presented in [5]. The modifications to the phantom presented in this work include additional inhomogeneous, high dielectric constant materials, representing the dense breast tissues. Each breast phantom is therefore composed of several different dense tissue materials, with dielectric constant ranging from 10 to 30. Different permittivity values were achieved by mixing TX151 and polythene powder with different amounts of water. In addition to inhomogeneous materials, the breast phantom includes a homogeneous skin, as well as normal breast tissue-equivalent liquid. The skin layer is 2 mm thick; it is a part of an 86-mm-radius hemisphere. When the skin phantom is fitted into the array, it lies 20 mm above the antenna elements. Electrical parameters of the skin layer are dispersive, and at 3 GHz, skin has a relative dielectric constant of about 35 and attenuation of 5 dB/cm. All developed phantom materials are dispersive with frequency-dependent characteristics similar to those presented in [8].

As already mentioned, studies from [1] have shown that MRI-based images can be considered quite realistic, regarding variation in dielectric properties of real breast tissues. In Fig. 2, we present an example of the contrast-enhanced MRI breast image. The malignant tumor tissue is visible on the right-hand side. Throughout the breast, we can also observe several small bright "objects" (e.g., glands, fibroconnective tissue, veins) with high water content (high dielectric constant and losses). Dark parts of the image suggest that a large part of the breast is composed of the fatty tissue with low water content. In the phantoms we have developed, we will use the high-permittivity (ϵ_r), inhomogeneous materials described above to approximate the dense, scattered tissue shown in Fig. 2. The normal breast tissue-equivalent liquid will serve as the replacement of fatty tissues in our experimental phantoms.

C. Imaging Scenarios

In Figs. 3–5, we present three different imaging scenarios, each with a different breast phantom, used to investigate the performance of the system in complex detection situations.

In the first imaging experiment (Fig. 3), a 40-mm dense inhomogeneous tissue, with $\epsilon_r = 27$ at 3 GHz, was placed right behind the nipple. The 7-mm-diameter spherical phantom tumor, with $\epsilon_r = 50$ at 3 GHz, was located at position $x = 30$, $y = 30$, $z = 30$ (units in [mm]). Position $x = 0$, $y = 0$, $z = -86$ corresponds to the position of the antenna in the center of the array. The remaining part of the breast phantom was then filled with the normal breast tissue equivalent liquid ($\epsilon_r = 10$ at 3 GHz).

In the second imaging experiment, the breast was assumed to consist of mainly dense tissue. Dense tissue ($\epsilon_r = 27$ at 3 GHz), shown in Fig. 4, was formed in the shape of a hemisphere. The 10-mm spherical phantom tumor was placed in contact with the dense tissue, which was then fitted into a solid shell with the same properties as the normal breast tissue-equivalent liquid. The solid shell was used to provide a 10-mm spacing between the skin layer and the dense tissue. This 10-mm gap, as well as a part above dense tissue, was filled with the normal breast tissue-equivalent liquid. This phantom has a clinical relevance since malignant tissue very often shows up right next to dense breast tissues.

In the third imaging experiment, shown in Fig. 5, the breast phantom interior was composed of two inhomogeneous dense materials with $\epsilon_r = 20$ and $\epsilon_r = 30$ (at 3 GHz), respectively. Both materials were deliberately made into very irregular shapes in order to approximate a real environment. Then, the 10-mm spherical phantom tumor was placed about 10 mm away from those dense materials. As was done previously, the remaining part of the breast phantom was then filled with the normal breast tissue-equivalent liquid. This breast phantom is probably the closest to the MRI breast image shown in Fig. 2.

III. Differential Imaging and Focusing Algorithm

Before applying the focusing algorithm, the tumor response must be extracted from measured data. Measured data contains the tumor response as well as additional undesired signals: antenna coupling, reflections from the skin, reflections from mechanical parts of the array. To subtract all the unwanted signals, we perform two measurements. The first measurement is performed with the array in a given position, then array is rotated (in a horizontal plane, around its central vertical axis) and a second measurement is recorded. Those two measurements are subtracted, resulting in a *differential* signal, which is used as an input into focusing algorithm. A detailed description of this method can be found in [6]. Because differential imaging method does not require a background measurement, it can be used in clinical scenarios.

A modified delay-and-sum (DAS) algorithm [5] is used to form 3D images of scattered energy. Essentially, the scattered energy at the given focal point $\vec{r}$ within the breast volume can be expressed as

$$F_e(\vec{r}) = \int_0^{\tau} \left(\sum_{i=1}^{M} \mathrm{CF}(\vec{r}) \cdot w_i(\vec{r}) \cdot y_i(t - T_i(\vec{r})) \right)^2 dt \quad (1)$$

where $M = N(N-1)/2$ (N is the number of antennas in the array), w_i is a location dependent weight calculated during preprocessing, y_i is the measured radar signal, and T_i is the time-delay. τ is the length of the integration window. The coherence factor $\mathrm{CF}(\vec{r})$ introduced here is a measure of the coherence quality of the received signals. CF has proved effective in ultrasound (US) imaging [9]. We define CF as

$$\mathrm{CF}(\vec{r}) = \frac{\left| \sum_{i=1}^{M} y_i(t - T_i(\vec{r})) \right|^2}{\sum_{i=1}^{M} \left| y_i(t - T_i(\vec{r})) \right|^2}. \quad (2)$$

Although in our experiments there is frequency dependence of the tissue losses and of the antenna radiation patterns, for simplicity we do not compensate for that dependence in our signal processing. Any attempts of a frequency-dependent compensation are questionable in practice because dispersion of tissues will be impossible to determine in heterogeneous breasts.

IV. 3D Imaging Results

To quantitatively assess imaging results, we introduce a measure of detection quality: ratio of peak clutter energy to a peak tumor energy (CT_{peak}), calculated within a full 3D image volume. Although all our results provide 3D data, only 2D results are presented for clarity in the following figures. Values in all presented images are normalized to 1. This is because the absolute pixel values after focusing do not provide any useful information using radar system.

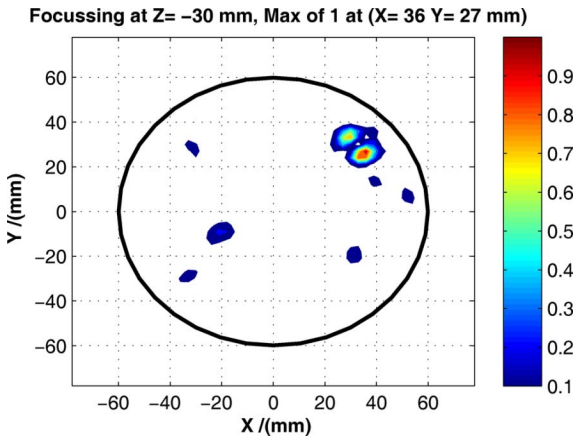

Fig. 6. 2D imaging results for experiment 1. $\mathrm{CF} = 1$ (coherence quality weighting not applied).

A. Imaging Experiment 1

Fig. 6 presents imaging results for the breast phantom shown in Fig. 3. We can clearly see the detected target (two lesions actually), in the correct position. Two lesions visible in the figure are due to the tumor signal extraction method by mechanical rotation of the array. This method is described in detail in [5] and [6].

CF was assumed to be 1 in the beamforming algorithm (1). The coherence quality weighting was not used since standard DAS already provided nice images. For the result from Fig. 6, the $CT_{\mathrm{peak}} = -5.4$ dB. After applying the CF weighting, this result (image not shown) was improved to $CT_{\mathrm{peak}} = -8.5$ dB.

B. Imaging Experiment 2

Fig. 7 shows imaging results for the breast phantom from Fig. 4. The dielectric contrast between tumor and the neighboring dense tissue is only 1.6:1. In spite of this challenging scenario, our imaging system was able to detect the target. Again, $\mathrm{CF} = 1$ was assumed during beamforming, resulting in $CT_{\mathrm{peak}} = -2$ dB. The higher CT_{peak} value, compared to the previous case, is not surprising due to the more complex breast phantom. After applying the CF weighting, this result (image not shown) was improved to $CT_{\mathrm{peak}} = -3.1$ dB.

C. Imaging Experiment 3

Imaging results for the most complex phantom investigated in this letter are shown Fig. 8. Results for the beamforming algorithm where $\mathrm{CF} = 1$ was assumed are presented in Fig. 8(a). The tumor phantom was comfortably detected. However, a higher clutter level than in the previous phantoms can be observed, and only $CT_{\mathrm{peak}} = -0.6$ dB was achieved. Clutter arises from heterogeneous structure of phantoms. Also, due to mechanical parts of the antenna array, skin layer, and

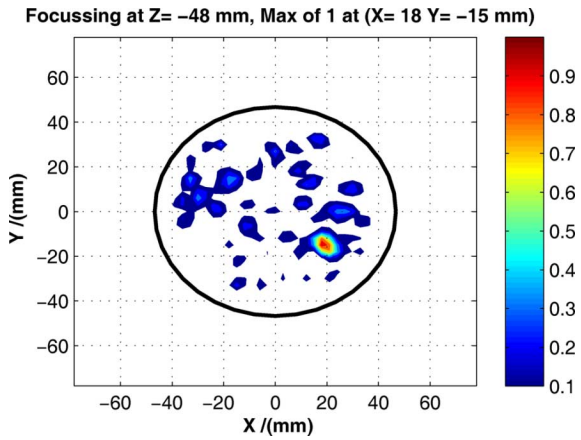

Fig. 7. 2D imaging results for experiment 2. $\mathrm{CF} = 1$ (coherence quality weighting not applied).

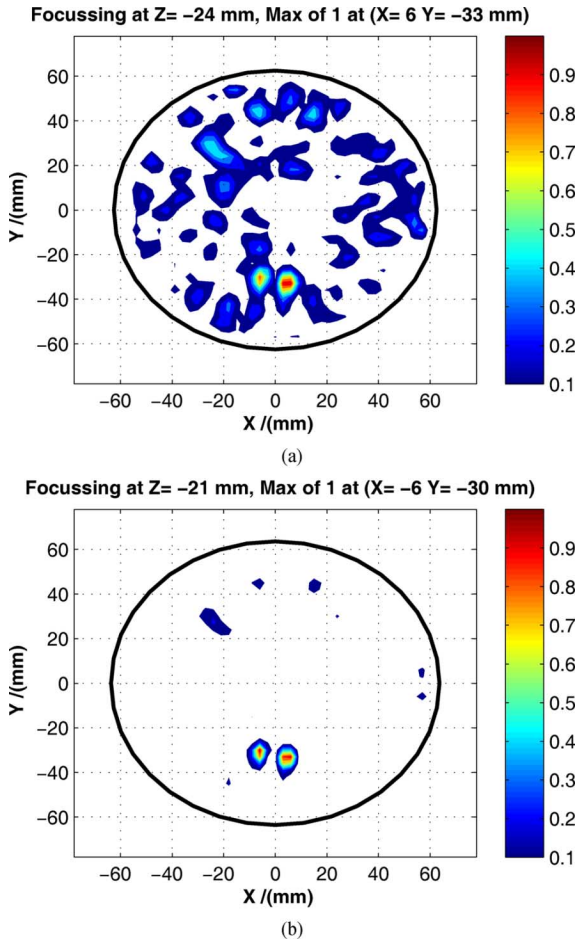

Fig. 8. 2D imaging results for experiment 3. (a) Results when $\mathrm{CF} = 1$ (coherence quality weighting not applied). (b) Results after the CF weighting was applied.

high-permittivity tissues, there are multiple pulses present in the imaging volume, which will contribute to the clutter.

Significantly better results were achieved when CF weighting was applied, providing $CT_{\mathrm{peak}} = -3.7$ dB. The resulting image is shown in Fig. 8(b). One can see that by using coherence quality weighting, most of the clutter was removed. The efficacy of the proposed new beamforming algorithm is indicated by this result.

V. Conclusion

The new results of the microwave radar imaging system for breast cancer detection were shown. Inspired by the recently published data on electrical properties of breast tissues, as well as MRI-based numerical breast models, we made three different highly inhomogeneous breast phantoms. Additionally, the new beamforming algorithm was proposed. In all three imaging scenarios, our radar system proved to be very efficient. Tumor phantoms were detected in all cases. For the most complex of all phantoms investigated in this letter, our new algorithm improved imaging performance from $CT_{\mathrm{peak}} = -0.6$ dB to $CT_{\mathrm{peak}} = -3.7$ dB.

The limiting factor in radar-based imaging is the heterogeneity of the breast. It is easier to detect even very small objects in homogeneous tissues than a high-contrast target embedded in heterogeneous tissues.

References

[1] M. Lazebnik, L. McCartney, D. Popovic, C. B. Watkins, M. J. Lindstrom, J. Harter, S. Sewall, A. Magliocco, J. H. Booske, M. Okoniewski, and S. C. Hagness, "A large-scale study of the ultrawideband microwave dielectric properties of normal breast tissue obtained from reduction surgeries," *Phys. Med. Biol.*, vol. 52, pp. 2637–2656, 2007.

[2] W. T. Joines, Y. Zhang, C. Li, and R. L. Jirtle, "The measured electrical properties of normal and malignant human tissues from 50 to 900 MHz," *Med. Phys.*, vol. 21, pp. 547–550, 1994.

[3] J. M. Sill, T. C. Williams, E. C. Fear, R. Frayne, and M. Okoniewski, "Realistic breast models for second generation tissue sensing adaptive radar system," in *Proc. 2nd Eur. Conf. Antennas Propag.*, Edinburgh, U.K., Nov. 2007, pp. 1–4.

[4] E. Zastrow, S. K. Davis, M. Lazebnik, F. Kelcz, B. D. Van Veen, and S. C. Hagness, "Development of anatomically realistic numerical breast phantoms with accurate dielectric properties for modeling microwave interactions with the human breast," *IEEE Trans. Biomed. Eng.*, vol. 55, no. 12, pp. 2792–2800, Dec. 2008.

[5] M. Klemm, I. J. Craddock, J. A. Leendertz, A. Preece, and R. Benjamin, "Radar-based breast cancer detection using a hemi-spherical antenna array—experimental results," *IEEE Trans. Antennas Propag.*, vol. 57, no. 6, pp. 1692–1704, Jun. 2009.

[6] M. Klemm, I. J. Craddock, A. Preece, J. Leendertz, and R. Benjamin, "Evaluation of a hemi-spherical wideband antenna array for breast cancer imaging," *Radio Sci.*, vol. 43, p. RS6S06, 2008.

[7] M. Klemm, I. J. Craddock, A. Preece, J. Leendertz, and R. Benjamin, "Microwave radar-based differential breast cancer imaging: Part 1 imaging in homogeneous breast phantoms and low contrast scenarios," *IEEE Trans. Antennas Propag.*, 2009, submitted for publication.

[8] J. Leendertz, A. Preece, R. Nilavalan, I. J. Craddock, and R. Benjamin, "A liquid phantom medium for microwave breast imaging," in *Proc. 6th Int. Congress Eur. Bioelectromagn. Assoc.*, Budapest, Hungary, Nov. 2003, p. 232.

[9] S.-L. Wang, C.-H. Chang, H.-C. Yang, Y.-H. Chou, and P.-C. Li, "Performance evaluation of coherence-based adaptive imaging using clinical breast data," *IEEE Trans. Ultrason., Ferroelectr., Freq. Control*, vol. 54, no. 8, pp. 1669–1679, Aug. 2007.